BUCKLING BEHAVIOUR OF LARGE GLARE FUSELAGE SHELLS UNDER COMPRESSION AND SHEAR LOADING

Peter HORST
Daimler-Benz Aerospace Airbus GmbH, Hamburg, Germany
Structural Repair Engineering
Kreetslag 10, 21129 Hamburg

Abstract

Two large fuselage panels made of the hybrid material GLARE® have been tested under both compression and shear loading. One panel represents a typical widebody crown panel, the other represents a window panel, including all doublers and the window frame. Both tests have been performed within the frame of the Brite/EuRam project BE2040: Composite Fuselage. While the frames and frame-skin connections of both panels are made of conventional aluminum 2024 T3, the bonded stringers are made of 7055 T7XX and the skin material is GLARE®3. The dimensions of both panels have been defined during extensive fuselage studies by means of the finite element method. The basic skin thickness is 1.4 mm. The load cases tested have been taken from a known realistic project. The tests have been performed at the shear-compression test set-up of Daimler-Benz Aerospace Airbus in Hamburg. Different load combinations have been tested. For both tests the loading led to global buckling and disintegration of the stringers as final state.

The paper summarizes the results of the tests, featuring special phenomena like the stress-strain behaviour at different locations, local and global buckling, and the way the stringer disintegration initiates the total failure of the panel. In addition, the results of the tests are compared with existing theoretical results. Different methods are used, ranging from simple analytical methods like Johnson-Euler to non-linear finite element methods. Results will be compared and interpreted. It can be shown that a number of results of the analytical methods fit very well, while others are not really satisfying. Special features resulting from the combination of a very flexible skin material (like the thin GLARE material) and a stringer material with a very high compressive yield strength are discussed.

1. Introduction

The recently developed glass fibre reinforced aluminium laminate material GLARE® is considered by some companies as a possible material for the fuselage and wing structure of aircraft in the near future. Essential weight savings and a better fatigue and damage tolerance are anticipated (ref. 1).

The objectives of two studies performed by Daimler-Benz Aerospace Airbus (DA) and in addition, work done in connection with the Brite/EuRam project 2040-Composite fuselage, have been the material selection, the definition of promising and necessary changes in design, a preliminary determination of new thicknesses for the envisaged components of a pressurized widebody aircraft fuselage and their consequences with respect to weight and costs of the aircraft.

In order to make sure that the studies have strictly been related to realistic questions, it has been decided to take details of design and loads from the Airbus A330 widebody aircraft. This aircraft type also served as basis of the comparison with the new GLARE® upper and side panel of the fuselage. Emphasis has been laid on the applicability of the new GLARE®-fuselage, taking into account all details of the initial design.

Only some structural elements of the fuselage have been chosen to be made of GLARE® in the studies. It has been decided to focus the interest on the upper (the crown) and side (window) shells of two sections of the Airbus A330, which may be taken as representative (fig. 1). These are the section 14, located in front of the wing and the section 17 behind the wing. Both sections have been chosen because they are long, highly stressed parts with different thicknesses within the panel (chemically milled/bonded doublers in the original version). In case of section 17 an additional spherical curvature is interesting with respect to manufacturing questions.

The chosen shells consist of seven panels each. The choice of these panels may be explained by the following points :

o the three upper shells of the fuselage structure are normally highly stressed in tension and are therefore susceptible to fatigue and crack propagation. Since GLARE® reveals very good features regarding damage tolerance, it seems to be reasonable to choose these shells.

o In addition, these panels are not mainly loaded by compression. Buckling is highly related to the

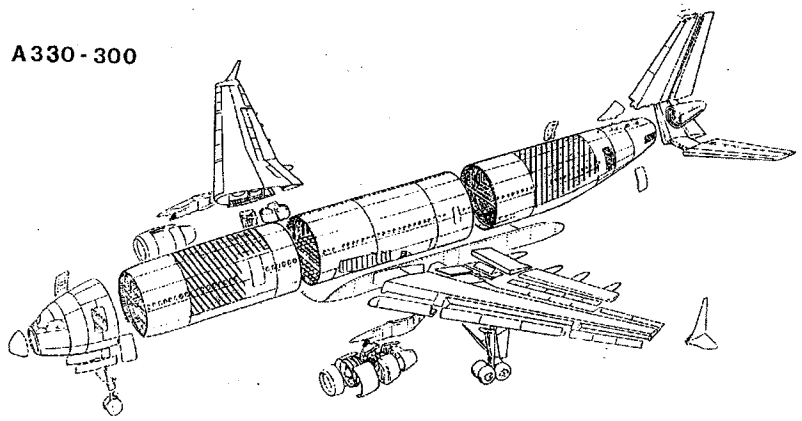

Fig. 1 : Parts considered in this study – Hatched areas covered by this study

Young's modulus, and this value is relatively low for GLARE®. As a matter of fact it turned out that, due to different loading conditions, also these panels may be loaded both in compression and shear.

o The two side panels (on both sides of each section) include the rows of windows. They are highly loaded by shear loads, therefore greater care has to be taken for buckling questions.

o The way stringers and frames are attached to the skin has also been studied.

It was not possible to undertake large parametric studies. Therefore, a set of realistic assumptions regarding the "optimal" configuration had to be made. It has been intended to search for a configuration of low weight, but bearable costs. Due to this assumption, it has been decided not to take GLARE® stringers and frames, in order to limit the material and manufacturing costs, although this would certainly result in lower weight savings.

The following configuration has been anticipated, but not all of theses points have been achieved; some had to be withdrawn :

o skin from GLARE®3

o deletion of bonded doublers of the basic design, where possible due to static and dynamic loading

o deletion of chemical milling

o deletion of titanium crackstoppers

o bonded stringers

o stringers from 7055

o better fatigue and damage tolerance behaviour of lap–joints.

It should be stated that this study has been performed by different departments of Deutsche Airbus, which are concerned with the following subjects : Static Strength, Weight, Fatigue and Damage Tolerance, Design, Design to Cost, Materials. Therefore, although a brought spectrum of interests has been considered, some aspects have been neglected, as e.g. the impact of a more flexible fuselage on loads etc..

The two shells tested with regard to buckling are a crown panel and a side panel of the rear section. Loads have been taken from this parts.

2. Features of GLARE® Material

GLARE® is a hybrid material made of two major components, first thin aluminum layers (0.2 to 0.4 mm thickness) and second UD–R–glass prepregs, which are bonded to each other. This kind of material shows some unique characteristics.

Most of the material data have been taken from publications. All of these data must be regarded as "typical" values and had to be reduced for the static justification. Some material data have been calculated according to some kind of compounding method, as it is common practice in laminate theory.

The basic material anticipated for this study is GLARE®3 using a 3/2 lay–up and a total thickness of 1.4 mm (three layers of 0.3 mm aluminium 2024 and two layers of UD–prepreg directed 0° and 90° to the L–direction of the aluminium sheet). Table 1 provides a brief survey of the material data needed to define the static behaviour of the material. As mentioned above, several data have been composed from basic data. (Please keep in mind that these data are estimated "minimum values"). For many cases the

blunt notch values have been used, instead of the ultimate values.

The calculation of the buckling behaviour needs some information about the elasto–plastic stress–strain relationship. As a first conservative guess this has been done for GLARE® – exactly in the same way as for monolithic aluminium – based on the Ramberg–Osgood equation. The Young's modulus of the prepreg has been regarded as constant. A curing temperature of 125°C has been adopted due to ref. 2. The difference of the operational temperature and the curing temperature result in a certain initial stress and strain state of the aluminium and glass layers, which has to be included in the calculation as a certain offset of the curves (see figure 2). The figure shows that GLARE exhibits a considerable hardening effect also beyond the yield strength.

From the values given in table 1 the following benefits of GLARE may be derived: a low density of the material, a good blunt notch stress and a high ultimate stress. All of these points are especially favorable for aircraft structures. Apart from these facts, further features are considerably good; e.g. the damage tolerance behaviour, the impact behaviour, the residual strength after impact and the burn–through behaviour. On the other hand the following drawbacks are found: the Young's modulus is about 25% lower, especially the shear modulus and the ultimate shear stress are rather small. Furthermore, the price of the material is rather high.

Parameter	Unit	GLARE3	2024 T3
E	MPa	57 477	73 000
G	MPa	18 450	27 000
ν	–	0.29	0.33
γ	g / cm^3	2.52	2.77
$\sigma_{0.2\,c}$	MPa	280.	290.
$\sigma_{0.2\,t}$	MPa	270.	290.
$\sigma_{ult.\,c}$	MPa	490.	440.
$\sigma_{ult.\,t}$	MPa	600.	440.
σ_{blunt}	MPa	450.	420.
$\tau_{ult.}$	MPa	175.	280.
$\varepsilon_{ult.t}$	–	0.047	0.12
$\varepsilon_{ult.c}$	–	0.025	0.12

Tab.1 : "Minimum" Static Values of GLARE3 (3/2 lay–up)
"c" for compressive, "t" for tension,
"blunt" for blunt notch, "ult" for ultimate and "0.2" for 0.002 remaining strain

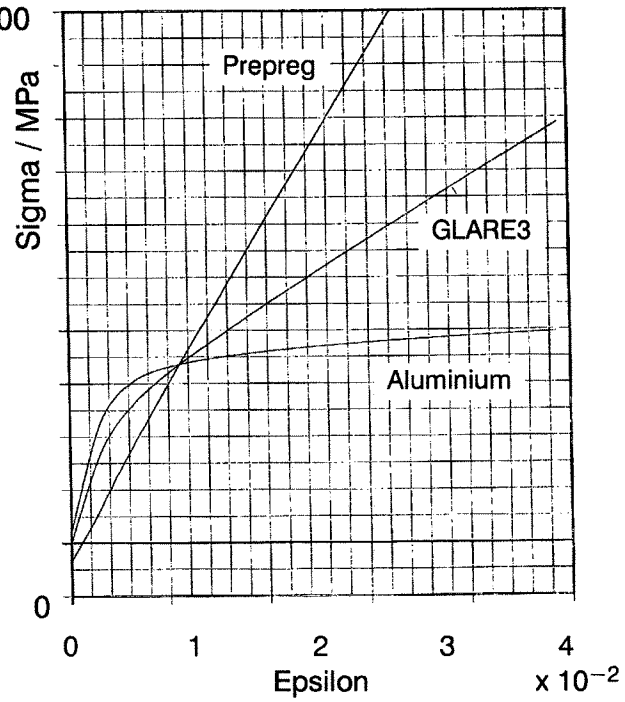

Fig. 2 : Stress–Strain–Relation of Glare Material and Components of GLARE3 3/2 Lay–Up

3. Description of Specimens

The two test specimen may be described as follows:

- a typical panel of the upper fuselage
- a typical panel of the window area.

Both have been tested in the DA test set–up for combined shear and compression loading. Obviously, the test set–up limits the desired dimensions of the test specimens, especially in the case of the window panel.

The principal designs of the specimens as well as the locations of the strain gauges are given in figure 3 and 4.

Both specimens have been tested in the DA test set–up for combined compression and shear loading, located in the DA test facility in Hamburg, Germany.

Loads can be applied by means of different hydraulic cylinders, for compression from the top and for shear by two cylinders, which apply shear forces into the horizontal and vertical edges.

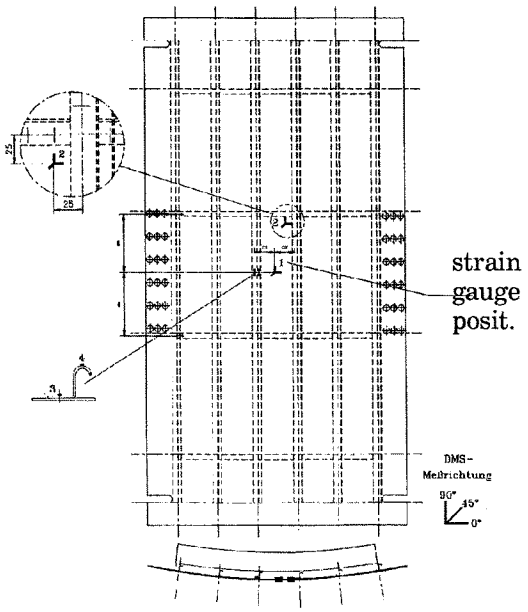

	1						2						3	4
	x	x	x				x	x	x				x	x
				x	x	x				x	x	x		
orientation	0	45	90	0	45	90	0	45	90	0	45	90	90	90
number	1	2	3	4	5	6	7	8	9	10	11	12	13	14

Figure 3: Design of Specimen 1

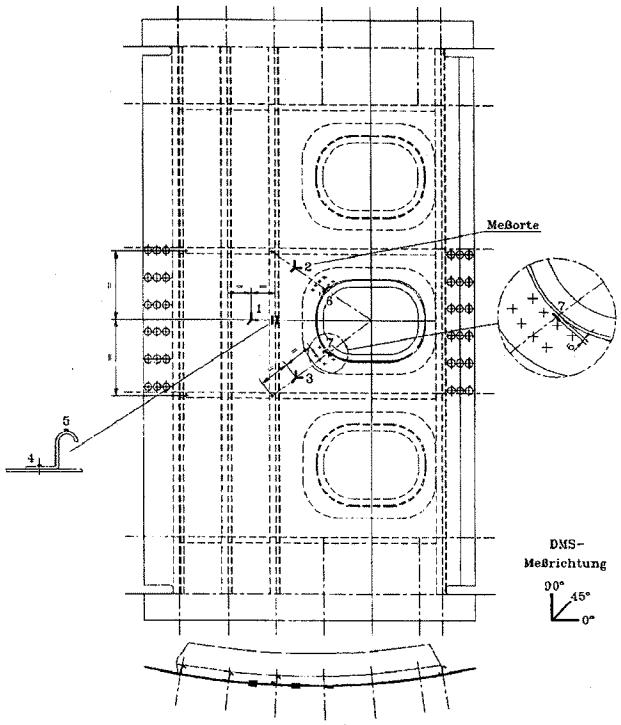

Figure 4 : Design of Specimen 2

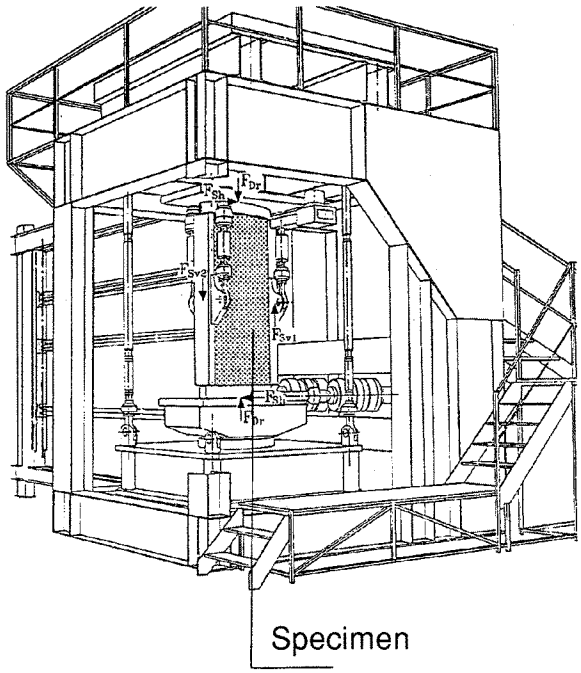

Figure 5: The Test Set–Up

The test specimen is clamped in a rig (see figure 5), which allows to introduce different shear and compressive loads independently. The shear loads are indicated by F_{Sh} and F_{Sv}, the compressive load by F_{Dr}. Normally both components of the shear introduction should be related to each other in a way which produces a regular shear stress, i.e. they should be related to each other in the same way as the length of the edges of the test specimen. The frames of the test specimen are constrained in the z–direction by means of some rods.

4. Results of the Crown Panel Test

The test has been performed with different load combinations, since the initial problem of pure compression – which is the ultimate load case for a crown panel – was not critical with respect to buckling. The different load combinations are given in table 2. In addition, figure 6 indicates the three shear/compression combinations, which have been used in the tests. Unfortunately, while the first sub–test did not result in remaining strains in the specimen, the further tests gave some remaining strains, which acted as imperfections for the further testing.

4.1 The first Sub–Test

This first sub–test reflects the way a crown panel is loaded with respect to buckling, i.e. pure compressive loading. Please note that buckling normally is not the criterion which governs the dimensions of a crown panel. Figure 7 shows the stress in the y–direction at the strain gauge location "1" (see figure 3) in the middle of the centre frame and stringer bay. Stresses from both sides, the inner and outer face of the skin

are shown. Due to small imperfections as well as a small eccentricity resulting from the stringers, a perfect buckling limit is not visible, but it becomes apparent that buckling occurs at a value slightly higher than j = 1.0. The first buckles were visible at about j = 1.2.

Subtest of the Shear–Compression Test # 1 (Panel of the Crown Area)

1st Sub–Test	Pure Compression	
	This is the real challenge of this panel !!!	
	ultimate load (j = 1,5)	= 130 kN
	0.66 * limit load	= 57.20 kN
	first local buckling	= 95.3 kN
	Further tests have been performed in order to assess, what the panel may be able to sustain.	
2nd Sub–Test	Shear – Compression with	
	$F_{Dr} / F_{Sv} = 10 / 1.4$	
	This test has been stopped when F_{Dr} was equal to 400 kN.	
	After complete unloading small remaining buckles were visible. These buckles acted as imperfection for the next test.	
3rd Sub–Test	Shear – Compression with	
	$F_{Dr} / F_{Sv} = 1.0 / 1.0$	
	First failure of the bonding between stringer and skin at	
	F_{Dr} = 386 kN F_{Sv} = 386 kN F_{Sh} = 238 kN	
	Global failure has not been anticipated in order to use the panel for some tests in conjunction with burn–through.	

Table 2 : External Forces

In addition, the theoretical buckling limits for the case of a perfect shell are shown. Both, the case of simply supported as well as clamped boundary conditions are given. It becomes obvious that the real buckling limit is very near to the clamped condition. This may be explained by the fact that the clips for the frame–skin connection, as well as the bonded stringers are relatively stiff. At j = 1.5 the buckling mode seems to be an almost classical scheme with two positive and two negative buckles per frame bay.

Figure 8 indicates that the stresses in the stringer remain quite low during the entire test up to j = 1.5. Also the bending moment is rather low, as it can be judged from the small difference in the stresses on top and at the bottom of the stringer.

The first sub–test has been stopped at j = 1.5. No remaining deformations have been found after the panels has been unloaded. This test has been performed with a complete clamping area. The compressive force which is consumed by the clamping area has been

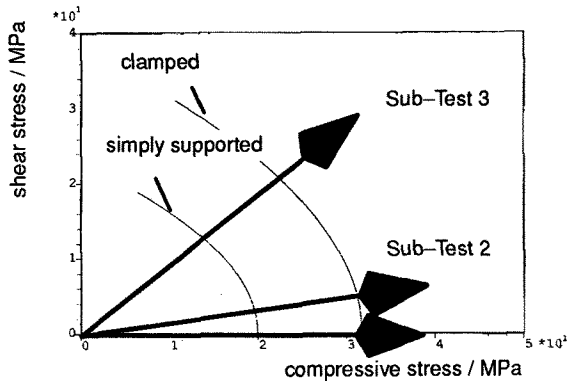

Figure 6: Shear / Compressive Stress Combinations in the sub–tests

taken into account linearily. This way may cause some problems in the higher post–buckling range, but it will not essentially affect the local buckling limit. Please note, that this procedure has been altered in sub–test 2. Some remarks concerning this point are given in section 4.2.

4.2 Further Sub–Tests : Here Sub–Test 2

4.2.1 Sub–Test 2a

Sub–test 2 has been performed twice. The shear/compression ratio was fixed at about 0.15. The difference is found in the following fact: while in sub–test 2a the clamped region remained as in the case of sub–test 1, this region has been altered by means of large holes. These holes provided a much higher flexibility. The higher flexibility of the clamped boundary region has the effect that a lower amount of the applied force is consumed by the clamped area. This is to say that the stress in the tested area much better matches the outer force.

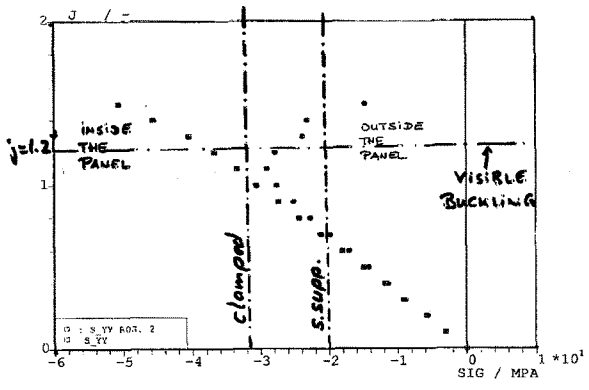

Figure 7: Stress σ_{yy} on both sides of strain gauge location 1 (sub–test 1)

Sub–test 2a has been loaded up to a compressive load of 40 to (400 kN). This is extremely high, compared

with j = 1.5 in sub−test 1, which was 136.5 kN.

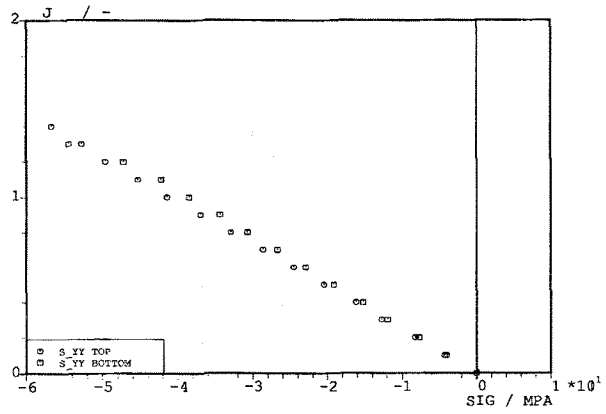

Figure 8: Stresses on top and at the bottom of the stringer (location 3 and 4)

Figure 9 and 10 show the stresses in the centre of the panels, both on the inside and outside. What is mainly interesting is the fact that very abrupt changes in the curves occur during loading. These changes signify changes in the buckling behaviour of the panel.

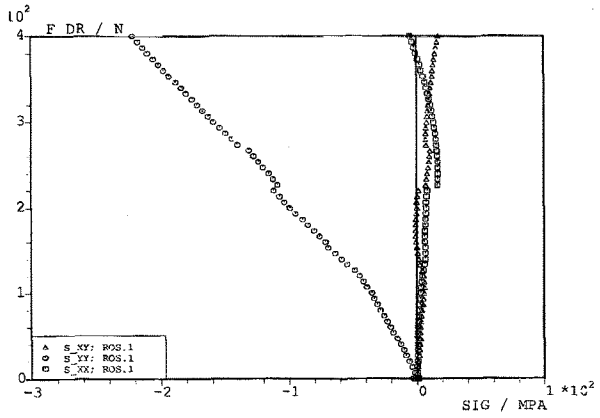

Figure 9: Stresses on the stringer side of strain gauge location 1 (sub−test 2a)

Figure 11 combines the results of sub−test 1 and subtest 2a. It is again the σ_{yy} component in the centre of the panel. Since both sub−tests have been performed without holes in the clamped boundary area, the stresses may be compared. The most interesting point seems to be that the local buckling limit is really only slightly influenced by the shear component, as it is foreseen in figure 6. The very good agreement of the curves in the lower loading range indicates that the assumption that no imperfections were produced during the sub−test 1 is right.
Figure 12 shows the stresses on top and bottom of the stringer at the strain gauge locations 3 and 4. Again, the stresses in the lower (prebuckling) range are very small and no bending moment can be seen. In the higher postbuckling range this changes significantly. Firstly, a considerable bending moment is found. Secondly, changes due to abrupt changes in the buckling mode may be seen easily. Thirdly, the stress at the bottom of the stringer almost reaches 400 MPa at 400 kN compressive loading. This shows that the material of the stringer has a major impact on the postbuckling area. The 7055 alloy provides such a high compressive strength that nothing happens. A stringer made of an other material, like e.g. 2024, would have failed already. Unfortunately, the first part of subtest 2 (called 2a) resulted in some remaining strains at unloading and hence in some small remaining buckles. These buckles acted like imperfections for the next test.

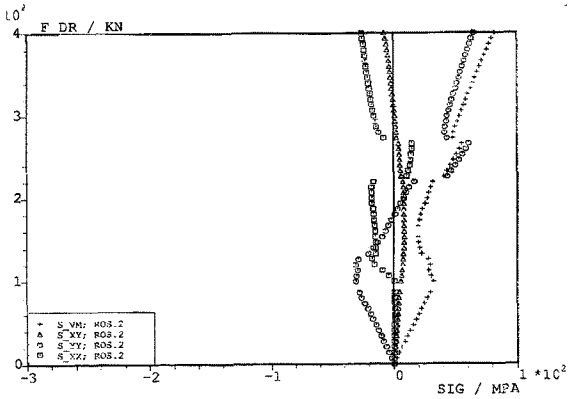

Figure 10: Stresses on the outer side of strain gauge location 1 (sub−test 2a)

4.2.2 Sub−Test 2b

Sub−test 2b initially is the same as sub−test 2a. The only differences are: the holes in the clamped boundary area and as a result of sub−test 2a, the imperfections which have been found after unloading in sub−test 2a.

Figure 13 compares the σ_{yy} stresses in the centre of the panel for both sub−test 2a and 2b. It is clearly visible that the imperfections from sub−test 2a influence the buckling behaviour at test 2b considerably. In addition, the stresses in the tested field are higher due to the application of the holes in the clamped area. This test is not very helpful in this sense.

Furthermore, the stresses in the stringer are shown in figure 14. Obviously, the stresses are somewhat higher than in sub−test 2a. The ratio of the stresses in both sub−tests may be used in order to assess the ratio of the stresses due to the application of holes in the clamping area. Obviously this ratio is getting

higher with increasing loads.

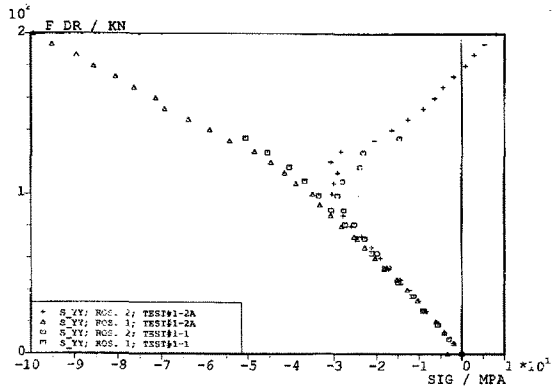

Figure 11: Stress σ_{yy} on both sides of strain gauge location 1
Comparison of sub–test 1 and sub–test 2a

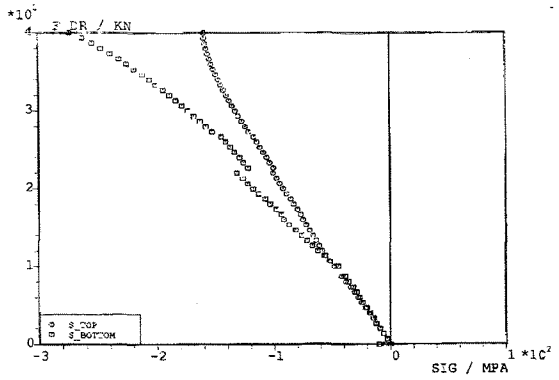

Figure 12: Stress on top and bottom of the stringer (location 3 and 4) (sub–test 2a)

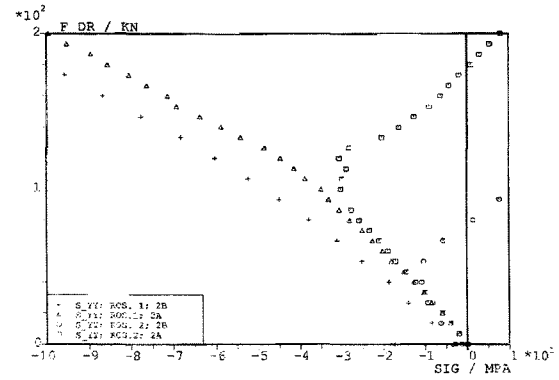

Figure 13: Stress σ_{yy} in the centre of the panel for sub–tests 2a and 2b

The figure 14 also indicates that the way buckles develop during loading is quite different in both sub–tests. While the first one shows rapid changes (probably indicating small snap–through effects), the second test shows very smooth changes. This effect may also be interpreted as the effect of imperfections.

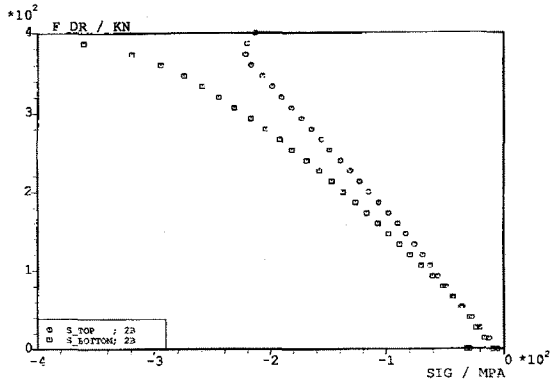

Figure 14: Stresses at the stringer for sub–test 2b

4.3 Further Sub–Tests: Sub–Test 3

In sub–test 3 the compressive and shear stresses have been chosen nearly equally.
It is quite obvious that the imperfections from sub–test 2 are even larger than the ones found after sub–test 2a alone. This sub–test 3 is therefore interesting only in two senses:

- The way the panel failed
- The stress level at which the panel failed.

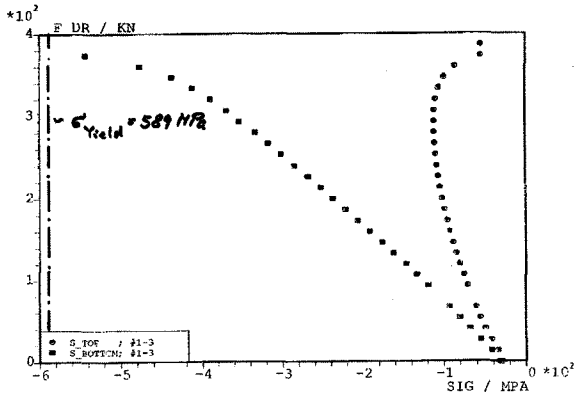

Figure 15: Stresses at the stringer for sub–test 3

Figure 15 shows the stresses at the strain gauge locations 3 and 4, i.e. on top and at the bottom of the stringer. The figure indicates that the imperfections were so large that heavy bending occurred from the start of the test.

Extremely high compressive stresses are found at the bottom of the stringer. The panel failed when the stringer approximately reached the nominal compressive yield strength of the material. It seems to be reasonable to assume that the strain location is not

exactly at the point where the highest stress occurred. Anyway, the moment of failure is very near to the point where the nominal compressive yield strength of 589 MPa is reached.

This shows that the compressive yield strength of the stringer material is of very high importance for the global failure of the panels. In the case of thin GLARE skin material the global buckling strength can be increased up to very high values, if a high strength stringer material is used. But it is obvious that the local buckling limit becomes critical in this case.

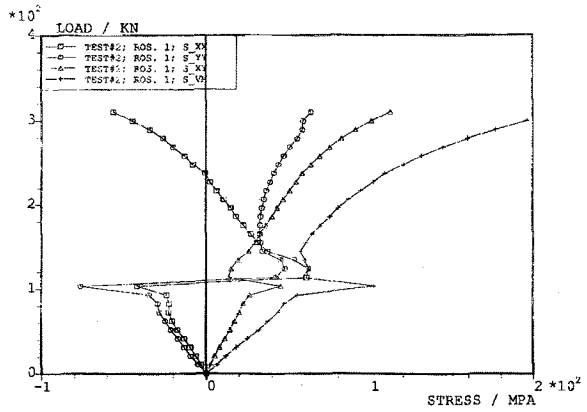

Figure 16: Stresses at strain gauge location 1 (internal face)

It seems to be very interesting that the bonding between skin and stringers is very good and lasts until the stringer itself is in the plastic range.

5. The window panel test results

The test has been performed using one single load combination. The axial compression at j = 1.5 is 155 kN, the shear force in the vertical direction is 144 kN. The test has been performed up to total failure of the panel. The strain gauge locations are given in figure 4. Three pairs of strain gauge rosettes are located at the internal and external face of the panel. In addition, strain gauges are located at one stringer and at the edge of the window cut-out.

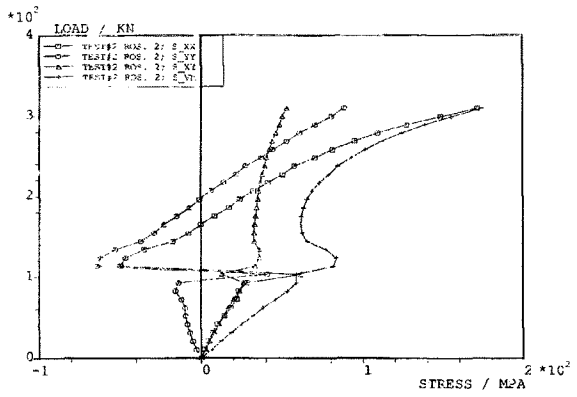

Figure 17: Stresses at strain gauge location 1 (external face)

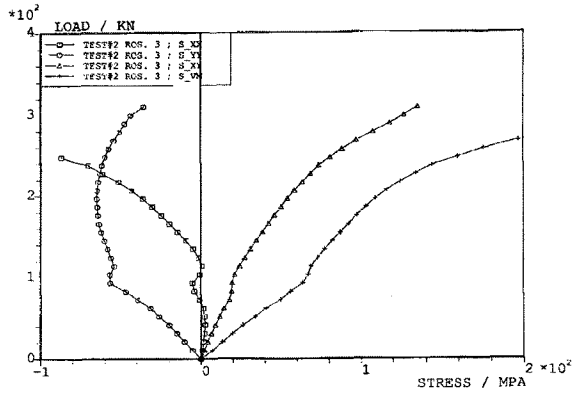

Figure 18: Stresses at strain gauge location 2 (internal face)

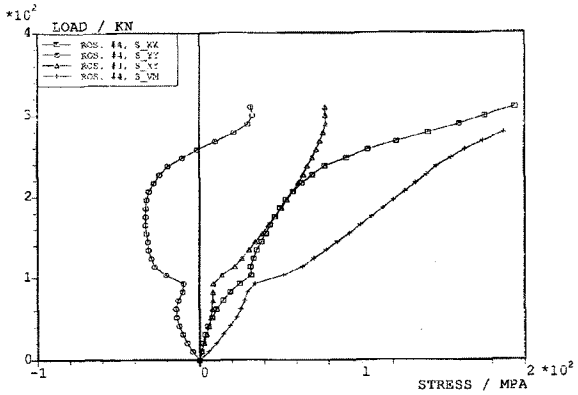

Figure 19: Stresses at strain gauge location 2 (external face)

The stress curves are given in figures 16 to 25. Figures 16 and 17 indicate the stress curves in the middle of the centre frame bay, which is still conventional. Two points can be derived from these figures: firstly, at about 0.65*j a rapid change in the stress distribution occurs. This indicates significantly that a major buckling effect occurs at this point. An interesting fact for this kind of structure can be observed by comparing the σ_{yy} stresses. Obviously, a slight bending effect occurs from the start. This can be interpreted in the way that the eccentricity of the panel lay-up allows not to speak of any initial local buckling limit.

It seems to be interesting that the finite element analysis showed a significant effect like this at j = 0.66. This would be a very nice coincidence. But, it seems not to be absolutely sure that the buckling effect in the test is purely related to the intended structural design. It may be possible that the buckling limit is also related to the fact that "dummy" window frames have been used in the two outer frame bays. These dummy window frames obviously did not show the bending stiffness of a normal window frame, and therefore produced an earlier buckling in this area. Secondly,

total failure occurred at about j = 3.0.

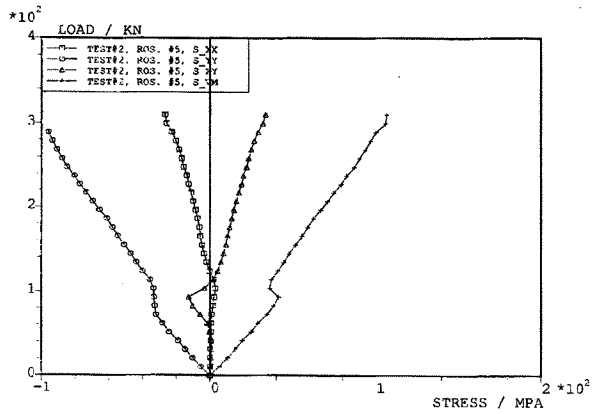

Figure 20: Stresses at strain gauge location 3 (internal face)

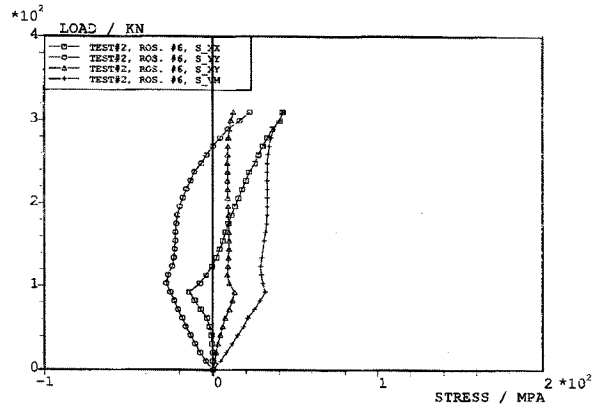

Figure 21: Stresses at strain gauge location 3 (external face)

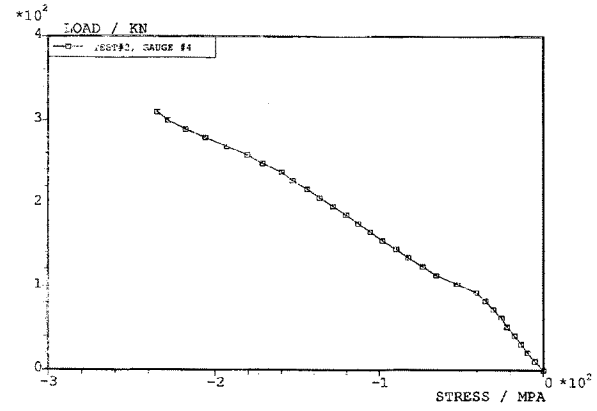

Figure 22: Stresses at strain gauge location 4

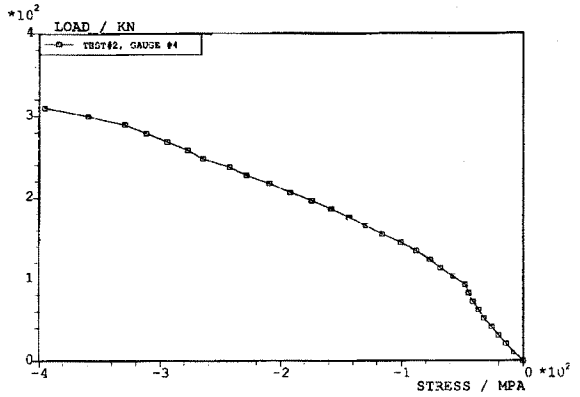

Figure 23: Stresses at strain gauge location 5

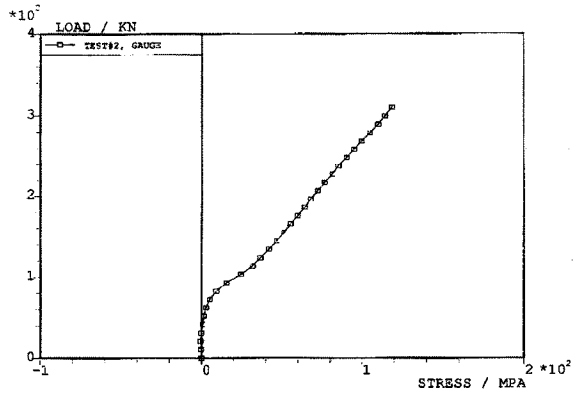

Figure 24: Stresses at strain gauge location 6

Figures 18 to 21 shows the stresses in the window part. Again it is obvious that bending occurred from the start. The buckling limit, which is given in figures 16 and 17 is not so clear anymore, although the effect of the snap−through in the adjacent field is still visible. It seems to be reasonable to assume that no real buckling occurred in this area.

Figures 22 and 23 gives the stresses on top and at the bottom of the stringer. The bending effect after the first real buckling limit at j = 0.65 is clear. It is quite clear that the maximum stress at failure of the panel is still far away from the yield strength of the stringer material. In this case a more global buckling of the entire panel seems to be the reason for the complete failure.

The figure 24 and 25, which show the stress at the edge of the window cut−out, indicate that the stresses in this region are very small, due to the large doublers in

this region. Therefore, a failure starting from this location seems not to be likely.

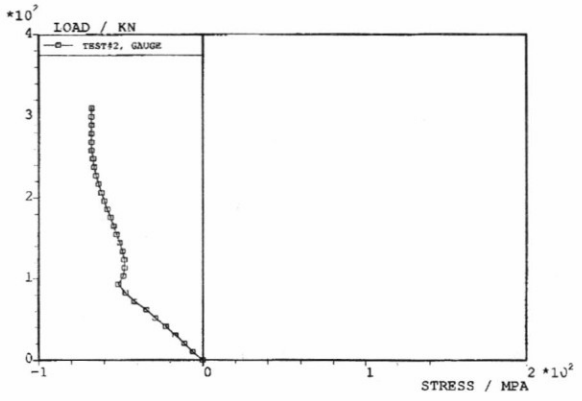

Figure 25: Stresses at strain gauge location 7

6. Finite Element Results

The window panel has been examined in a buckling analysis by means of an ANSYS non–linear finite element analysis. Three kinds of loading conditions have been tested : pure compression, pure shear and combined loading (using a mixture of shear and compression

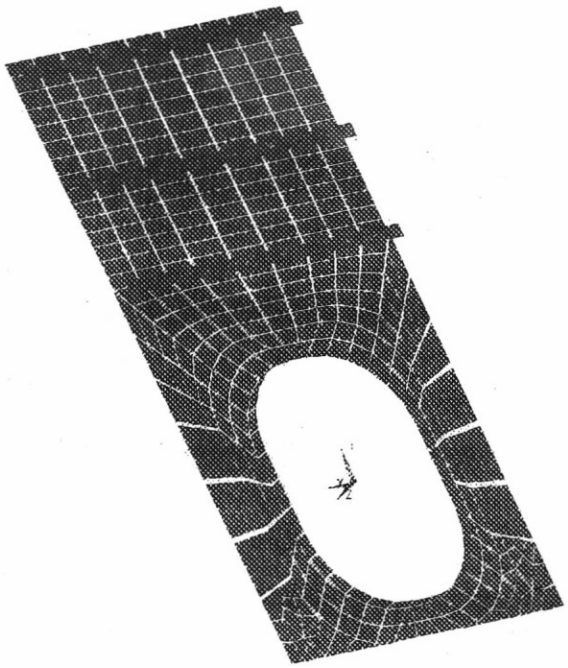

Figure 26 : FE – Mesh

The principle finite element mesh is shown in figure 26. This mesh represents one frame bay of the test specimen, i.e. the actual test region. Due to the fact that the incorporation of forces is quite complicated for stiffened panels, it has been chosen to introduce loads by means of boundary conditions. This method does of course mean that for combined loading the mixture of the loads is nearly fixed. But it seems that this is nearly true in this case. The mesh is relatively rough for a thorough non–linear analysis, especially in the region of the pure shear panels and the stringers, but it seems to be sufficient for a first estimation.

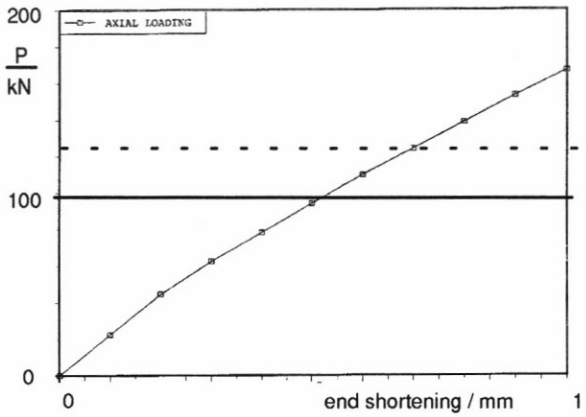

Figure 27: Load–Displacement Curve for Compressive Loading

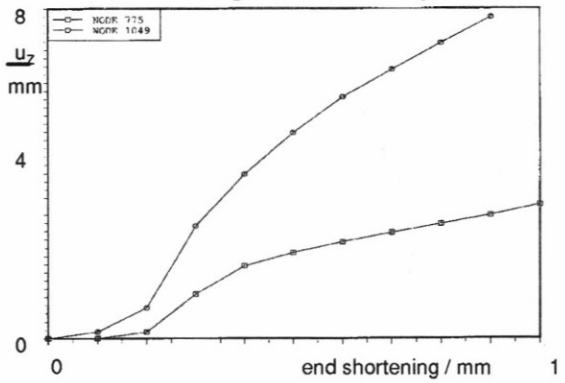

Figure 28: Deflection over End–Shortening

The basic buckling behaviour of the panel under pure compression as shown in figure 26 is indicated in figure 27. Two points are crucial in this case: the non–linearity after only a low loading of about 40 kN, the fact that the compressive loading in the case of the combined loadcase is about 122 kN (indicated by the dotted line). The first point may easily be explained by the fact that local buckling occurs in the two upper shear fields. This actually does not alter the overall stability of the panel. The second point is mainly interesting with regard to the combined loading case, since it seems to be interesting to use the related value of the end shortening for the combined loadcase.

Figure 28 gives a good summary of the buckling behaviour, the deflection u_z is plotted versus the end shortening for two discrete nodes: the middle of the upper

shear field (node 775) and the edge of the window frame (node 1049)

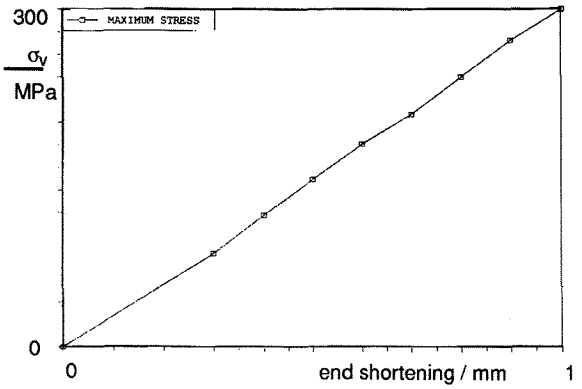

Figure 29 : Maximum Stress in the Stringer at Compressive Loading

It can be concluded again that the first buckling occurs below an end shortening of 0.2 mm, although it appears that node 1049 shows an out of plane displacement in the linear case, due to the asymmetric lay–up of the region. The maximum stress (v.Mises) is plotted in figure 29. This stress mainly occurs in the stringers. It obviously is far below the maximum allowable for the 7055 alloy. In addition, the upper flange of the stringer is not very well modeled and will therefore result in a lower local stiffness of the model compared with the real stringer.

The shear loaded calculation has only been made in order to assess the right ratio of shear and compressive displacements.

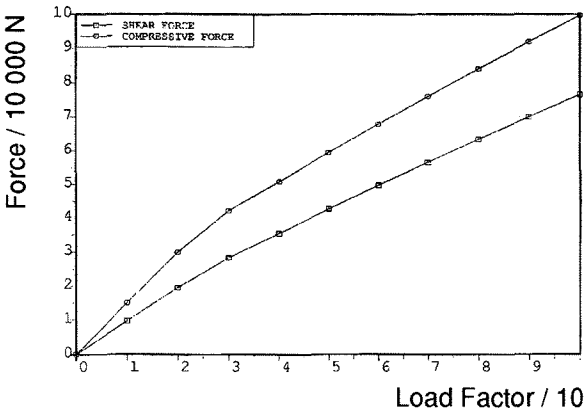

Figure 30: Compressive and Shear–Load versus Load Factor

In the case of combined loading figure 30 shows the compressive and shear load plotted versus the load factor, where the load factor of 1 indicates the compressive and shear deformation, which has been calculated in the last section for the ultimate load in the case of the combined loadcase. From this plot three points may be derived:

First, the actual ultimate load has not been reached in this calculation, due to the combination of the two load cases. But, since the the actual panel is curved, and this has not been taken into account in this finite element model, this seems to be balanced. Second, local buckling occurs relatively early in the load history. Third, a global failure of the structure is not likely to occur during loading.

Conclusions

The essential problem in the case of thin GLARE panels is the local buckling behaviour of the skin material, provided that stringer and skin–stringer connection are well developed, i.e. that the stringer pitch may be influenced by many additional criteria like fatigue and damage tolerance, manufacturing and the design of the skin frame connection, and is therefore not optimized in a way that global and local buckling are likely to occur at the same time.

The theoretical means for the assessment of local and global buckling seem to be sufficient.

Acknowledgement

The author gratefully acknowledges the financial support of a larger part of the work by the BRITE/EURAM project BE2040.

References

[1] Horst, P. ; Ohrloff, N.
"Possible Applications of GLARE Material as shown by the Example of the Airbus 330", Proc. of the Deutscher Luft–und Raumfahrt–Kongress 1994, pp. 591 – 601

[2] Verolme, J.L.
"The Compressive Properties of GLARE", TU Delft, Delft, 1991